

# Particle production in HRG with thermodynamically consistent EoS and partially deformable hadrons

Sameer Ahmad Mir,<sup>\*</sup> Iqbal Mohi Ud Din, Nasir Ahmad Rather, and Saeed Uddin<sup>†</sup>  
*Department of Physics, Jamia Millia Islamia, New Delhi, 110 025, India*

M. Farooq Mir  
*Department of Physics, University of Kashmir, Jammu and Kashmir, 190 006, India*  
(Dated: June 18, 2024)

In the present work, we analyze several strange as well as non-strange relative hadronic yields obtained in the ultra-relativistic heavy-ion collisions (URHIC) experiments over a wide range of centre-of-mass collision energy ( $\sqrt{s_{NN}}$ ). We invoke the formation of a hot and dense hadronic resonance gas (HRG) in the final stage following the URHIC. We use an earlier proposed thermodynamically consistent approach for obtaining the equation of state (EoS) of a hadronic resonance gas (HRG). It takes into account an important aspect of the hadronic interaction, viz., the hadronic hard-core repulsion, by assigning hard-core volumes to the hadrons, leading to an excluded volume (EV) type effect. We have invoked the bag model approach to assign hard-core volumes to baryons (antibaryons) while treating mesons to be point particles. We employ ansatz to obtain the dependence of the temperature and baryon chemical potential of the HRG system on the centre-of-mass energy in the URHIC. We also find strong evidence of double freeze-out scenario, corresponding to baryons (antibaryons) and mesons, respectively. Strangeness (anti-strangeness) imbalance factor is also seen to play an important role in explaining the ratio of strange hadrons to the non-strange ones. The HRG model can explain the experimental data on various relative hadronic multiplicities quite satisfactorily over a wide range of  $\sqrt{s_{NN}}$ , ranging from the lowest RHIC energies to the highest LHC energies for the set of the model parameters obtaining the best theoretical fit to the experimental data by minimizing the  $\chi^2/\text{dof}$  value.

PACS numbers: 05.70.Ce, 12.38.Mh, 12.39.Ba, 13.30.Eg, 13.75.Cs, 24.10.Pa, 24.85.+p, 25.75.-q, 25.75.Dw

## I. INTRODUCTION

The study of hadronic and nuclear collisions at ultra-relativistic energies constitutes a highly focused subfield of high-energy physics. The ultra-relativistic heavy-ion collisions (URHIC) provide immense potential to investigate the fundamental constituents of matter i.e., quarks and gluons, and the complex forces governing their interactions. The energy densities obtained by colliding high-energy nucleus beams in a laboratory environment are significant enough to enable the transformation of strongly interacting matter, where hadrons are the fundamental degrees of freedom, with quarks and gluons confined inside various hadronic species, to a state where quarks and gluons themselves become the fundamental degrees of freedom due to the melting of hadrons in an environment of high temperature and density. Existence of such a state is predicted by quantum chromodynamics (QCD), which is the fundamental SU(3) gauge theory of strong interactions [1]. In this altered state, also known as quark-gluon plasma (QGP) [2–6], the quarks and gluons are de-confined over an extended region, spreading over almost the entire physical volume of the system initially formed. As particles are continuously produced within the QGP, which continuously expands in the outward direction, the density and temperature drop to a critical level where quarks and gluons can no longer remain free due to the highly non-perturbative nature of the strong force. Consequently, the system under-

goes a process called hadronization, where quarks and gluons are again confined and hadrons are produced. These hadrons continue to interact and produce more hadrons until a certain stage where a chemical freeze-out (CFO) occurs. The term “chemical freeze-out” refers to the stage of the evolving strongly interacting matter (SIM) after the collision, where particle “composition” becomes fixed or frozen in time and the system is no longer undergoing any significant changes in terms of particle creation and annihilation.

Therefore, URHIC presents a unique and crucial opportunity for investigating the properties and behaviour of the SIM under extreme conditions of temperature, pressure and density. The abundant production of various hadronic species in these URHICs has been extensively studied in the framework of statistical thermal models. Though the dynamics governing the evolution of the system are quite complex, the system is expected to reach a reasonably high degree of chemical and thermal equilibrium [7, 8]. Under this condition, the properties of the system leading to the production of particles in the final state of the system before its breakup can be described using statistical models with temperature ( $T$ ) and baryonic chemical potential ( $\mu_B$ ) as two important independent free model parameters [9–17]. It is worthwhile to note that the baryon chemical potential is also an indicator of the excess of baryons over antibaryons in the system.

In other words, this description assumes the emission of particles from a source that is not only thermally but also chemically well equilibrated, a state that is created by the inelastic particle reactions under specific conditions within the system. The statistical model parameters defining the chemical freeze-out stage of the colliding system are determined by

<sup>\*</sup> sameerphst@gmail.com

<sup>†</sup> suddin@jmi.ac.in (Corresponding Author)

the actual yield of the produced hadrons.

Following the CFO, the particles in the dense system continue to interact elastically, leading to its expansion and further cooling until they stop interacting with one another. This stage is called kinetic freeze-out (KFO), where the particle's "distribution in momentum space" gets frozen in time [18–20]. The two freeze-outs, CFO and KFO, essentially occur when the mean free paths of the particles, for inelastic and elastic reaction, respectively, in the system become comparable to its overall physical size.

The ideal hadron resonance gas (Id-HRG) model is a phenomenological framework providing an equation of state (EoS) that has been used extensively to analyse many experimental hadron yield data from ultra-relativistic heavy-ion collisions (URHIC). This straightforward approach has produced fairly good descriptions of experimental data over a broad range of energies, ranging from SchwerIonen-Synchrotron (SIS) to the Relativistic Heavy-Ion Collider (RHIC) at BNL and further to the highest energies of the Large Hadron Collider (LHC). These studies have enriched our broad understanding of such states to a great extent [21–23].

The Id-HRG model's ability in the temperature range of  $T \sim 100 - 150$  MeV and at negligible as well as finite baryonic chemical potentials ( $\mu_B$ ) at CFO indicates that it can provide a useful and simple phenomenological framework for reproducing the various hadronic yields, which are otherwise a complex phenomenon seen in the lattice QCD calculation [24–27].

However, some deviations from the Id-HRG models are anticipated. The exploration of extensions beyond the Id-HRG framework has been the centre of attention. In particular, the excluded volume-based hadronic resonance gas, i.e., the EV-HRG model, has been studied in depth [28–30]. The EV-HRG model mimics the repulsive interactions among hadrons at short distances [30–36].

The van der Waals (vdW) model [37–39] has been proposed as an extension in this direction that takes into account both repulsive as well as attractive interactions between hadrons. Within the general framework of lattice Quantum Chromodynamics (lQCD), repulsive interactions have recently received attention, with emphasis on conserved charges. A basic feature of heavy-ion collisions can be the conservation of charge, which includes different conserved variables like strangeness (S), electric charge (Q) and baryon number (B). These quantities can be equivalently expressed in terms of "net" number of up, down and strange quarks in the system. The electric charge is mostly distributed among the pions, as they are the lightest hadrons and are copiously produced in the collision process at a later stage which further increases with the collision energy. On the other hand, strangeness is mostly produced in the earlier stages of the collision [40–45].

It has also been shown that the absence of repulsive interactions in the hadronic EoS restricts the construction of a first-order quark-hadron phase transition within the Bag model approach [46] according to the Gibbs criteria across the entire  $T - \mu_B$  plane. The short-range repulsive hard-core interactions between a pair of baryons or antibaryons is incorporated using a phenomenological approach in the excluded volume

inspired HRG models [47–57].

In several theoretical calculations, the baryons in the system are generally assumed to be incompressible. Moreover, they have been considered either completely non-deformable spherical objects or fully deformable objects under extreme conditions of high density where they can acquire any other shape but with the same volume due to their non-compressibility. The outcome of these two apparently extreme and opposing assumptions is that for baryons (or antibaryons) in the system having radius  $r$ , the amount of excluded volume due to each baryon (or antibaryon) in the former case becomes  $(16/3)\pi r^3$  [58, 59] while in the latter case it turns out to be  $(4/3)\pi r^3$  [60].

It is important and interesting to understand that how systems consisting of hot and dense hadronic gas can behave when formed in the most central heavy-ion collisions over a wide range of centre of mass collision energy,  $\sqrt{s_{NN}}$ . Here, it may be worthwhile to realize how the properties of such system's can be affected by the different collision energies. There is strong experimental evidence that, towards smaller collision energies, the colliding nuclei are able to stop each other completely. However, as the centre of mass frame energy of the colliding beams of heavy nuclei increases beyond the SPS energy, i.e.,  $\sqrt{s_{NN}} \sim 17.3$  GeV per nucleon, the nuclear transparency effects set in. At this as well as the low RHIC energies, this effect turns out to be partial but as the energy is further increased, the nuclear transparency effect tends to become more prominent. The main outcome of this effect is that at low and intermediate energies, the system that is formed due to the high degree of stopping in nuclear collisions contains almost all the colliding (participating) nucleons in the most central collisions, along with other hadrons (mostly pions, which have a zero baryon number) in the bulk system. Hence, a baryon-rich system is formed, which maintains a large baryon chemical potential. On the other hand, at sufficiently large collision energies, as a result of the nuclear transparency effect setting in, the bulk of the system is formed in the region between the two receding nuclei due to the highly excited vacuum. Consequently, the system is almost baryon-symmetric, which maintains a small chemical potential. Hence, with increasing collision energy, this effect becomes more prominent and the systems formed in URHIC tend to maintain smaller chemical potentials. It is found in experiments that though there is a rapid increase in the thermal temperature of the system as the energy is increased from a reasonably low value of  $\sqrt{s_{NN}}$ . However, it tends to almost saturate towards very high collision energies at RHIC and LHC [61–63].

The final state relative hadronic yields obtained from these experiments are known to depend very sensitively on the energy of the colliding beam nuclei. Hence, there are strong indications that the relative hadronic yields might serve as an important tool to explore the properties at the chemical freeze-out (CFO) of the hot and dense system formed at various collision energies. One can therefore expect that within the framework of the EV-HRG model as well, one can establish a correlation between the thermal parameters of the system and the relative yields of various hadronic species.

Therefore, in this work, our aim is to use a realistic phenomenological EoS such that it can describe the relative hadronic yields over a wide range of collision energy and hence extract reasonable values of various model parameters. We will also attempt to understand of the impact of the finite baryon sizes on hadronic yields, which lead to excluded volume type effect in the system, as already discussed above. In addition, we will explore how the consideration of incompressible but *partly* deformable baryonic (antibaryonic) states can affect the relative particle yields. We shall also apply various conservation criteria, such as strangeness and electric charge conservation, in the system during its evolution till the CFO. The study of energy dependence of these quantities, along with other model parameters, can shed light on the behaviour of the systems formed at different collision energies as they approach the chemical freeze-out stage.

This paper is structured as follows: In section II, we present a brief overview of the excluded volume hadron resonance gas (EV-HRG) model. In section III, obtained results are discussed in depth. Finally, we summarise and conclude our results in Section IV.

## II. THE STATISTICAL APPROACH

The Ideal Hadron Resonance Gas (Id-HRG) model is a statistical-thermal framework utilized to describe the properties of a system regarded as a hot and dense gas of various hadronic species that are considered to be in a state of thermo-chemical equilibrium [64]. It aims to help us understand the macroscopic properties of the system by incorporating the statistical behaviour of microscopic constituents i.e., hadrons. The hadrons within the system continue to interact inelastically until freeze-out, hence their numbers are not conserved. Under this condition, a grand canonical partition function-based EoS assuming thermal distribution functions for the constituent hadrons of the system is a suitable way to compute various thermodynamical quantities for a HRG system. This can also provide hadronic yields seen in URHIC.

The hadronic EoS within the framework of statistical models has also been employed through various computational tools like THERMUS [65], Thermal-FIST [66], and THERMINATOR [67]. These authors have calculated several thermodynamic parameters of the system.

As discussed in Section I, the hard-core repulsion is an essential feature of the hadronic interaction at short distances, which is assumed to act between a pair of baryons or a pair of antibaryons [47, 50]. Hence, in a system at sufficiently high densities, the mean separation between its constituents becomes small enough, and the effect of the short range repulsive interaction becomes important. In a simplistic approach, it is assumed that a given baryon in the system cannot move freely over the entire volume of the system but only in the *available* volume, which is free from other baryons. Hence, an effective proper volume  $v_0$  is assigned to every baryonic species. Following van der Waals' excluded volume (EV) type treatment and for a system with  $N$  number of particles, the volume  $V$  is replaced by  $V - v_0 N$  [68]. However, in a strict

sense, the procedure is thermodynamically inconsistent. For example, the net baryon density ( $n_B$ ) of the system calculated from the grand partition function or thermodynamic potential ( $\Omega$ ) cannot be derived as  $n_B \neq \partial\Omega/\partial\mu_B$  [47, 49, 50, 69].

Several models have emerged to rectify these inconsistencies by offering varied perspectives and solutions. In this context, a thermodynamically consistent EoS formulation of the EV-HRG was developed by Rischke et al. [51]. In this approach, strong repulsive interactions exist between all pairs of baryons and all pairs of antibaryons [70–73] while the interactions between baryon-antibaryon pairs are only attractive in nature and can lead to annihilation processes [70, 74, 75]. Similarly, the strong meson-meson and meson-(anti)baryon interactions are also predominantly of an attractive nature.

The EV-HRG model proposed by Rischke et. al. can be viewed as an extension of the Id-HRG model [51]. It is expected that thermodynamically consistent EoS can provide a more reasonable understanding of the behaviour of nuclear matter under extreme conditions of temperature and densities. In the following, we first briefly review the grand canonical ensemble (GCE) based formulation for an Id-HRG consisting of point particles.

The expression for the partition function of the  $i^{\text{th}}$  particle specie can be written as [64, 74, 76]

$$\ln \mathcal{Z}_i^{\text{id}}(T, \mu, V) = \frac{V g_i}{2\pi^2} \int_0^\infty p^2 dp \ln \{1 \pm e^{-(E_i - \mu_i)/T}\} \quad (1)$$

where + sign corresponds to fermions and anti-fermions, while the - sign corresponds to bosons. The quantities  $g_i$  and  $E_i = \sqrt{p^2 + m_i^2}$  are respectively the spin-isospin degeneracy and energy of the  $i^{\text{th}}$  hadronic specie.  $V$  is the physical volume of the system and  $\mu_i$  denotes the chemical potential of  $i^{\text{th}}$  specie which is defined as

$$\mu_i = B_i \mu_B + S_i \mu_S + Q_i \mu_Q \quad (2)$$

where  $B_i$ ,  $S_i$ , and  $Q_i$  are the baryon number, strangeness, and electric charge of the  $i^{\text{th}}$  hadronic specie. The quantities  $\mu_B$ ,  $\mu_S$ ,  $\mu_Q$  are represented as baryon chemical potential, strange chemical potential and electric chemical potential, which control the net baryon, net strangeness and net electric charge content of the system, respectively.

Using the grand canonical partition function  $\mathcal{Z}_i^{\text{id}}(T, \mu_i, V)$ , one can get the pressure  $p_i^{\text{id}}(T, \mu_i)$  and number density  $n_i^{\text{id}}(T, \mu_i)$  as:

$$\begin{aligned} p_i^{\text{id}}(T, \mu_i) &= \lim_{V \rightarrow \infty} T \frac{\ln \mathcal{Z}_i^{\text{id}}(T, \mu_i, V)}{V} \\ &= \frac{T g_i}{2\pi^2} \int_0^\infty p^2 dp \ln \{1 \pm e^{-(E_i - \mu_i)/T}\} \quad (3) \end{aligned}$$

$$n_i^{\text{id}}(T, \mu_i) = \left( \frac{\partial p_i^{\text{id}}}{\partial \mu_i} \right) = \frac{g_i}{2\pi^2} \int_0^\infty \frac{p^2 dp}{1 \pm e^{-(E_i - \mu_i)/T}} \quad (4)$$

The entropy density, represented as  $s_i^{id}$ , is determined as  $s_i^{id} = (\partial p_i^{id} / \partial T)_{\mu_i}$ . Meanwhile, the energy density  $\epsilon_i^{id}$ , which can be derived from another thermodynamical relation  $\epsilon_i^{id}(T, \mu_i) = T s_i^{id}(T, \mu_i) - p_i^{id}(T, \mu_i) - \mu_i n_i^{id}(T, \mu_i)$ , is written as [77]

$$\epsilon_i^{id}(T, \mu_i) = \frac{g_i}{2\pi^2} \int_0^\infty \frac{p^2 dp}{1 \pm e^{-(E_i - \mu_i)/T}} E_i \quad (5)$$

One can also write the ideal grand canonical partition function  $\mathcal{Z}_{GC}^{id}(T, \mu_i, V)$  for any hadronic specie in terms of the corresponding canonical partition function as

$$\mathcal{Z}_{GC}^{id}(T, \mu_i, V) = \sum_{N=0}^\infty e^{\mu_i N/T} \mathcal{Z}_C^{id}(T, N, V) \quad (6)$$

Here  $\mathcal{Z}_C^{id}(T, N, V)$  denotes the canonical partition function for a system consisting of  $N$  particles at temperature  $T$  and volume  $V$ . As discussed above, the grand partition function, which incorporates baryonic repulsive interactions, can be obtained by assigning a finite size to all baryons (antibaryons). This, as discussed in section I, results in an excluded volume effect where a hard-core volume  $v_0$  is assigned to each baryon. Thus, for a single component system ( $i^{th}$ ) having  $N$  number of finite size particles, the volume  $V$  in the ideal canonical partition function is replaced by the volume available to any given baryon in the system, i.e.,  $V - v_0 N$ . This leads to a modified grand canonical partition function incorporating the effect of repulsive interaction as follows

$$\mathcal{Z}_{GC}^{excl} T, \mu_i, V) = \sum_{N=0}^\infty e^{\mu_i N/T} \mathcal{Z}_C^{id}(T, N, V - v_0 N) \theta(V - v_0 N) \quad (7)$$

The canonical partition function  $\mathcal{Z}_C^{id}(T, N, V - v_0 N)$  thus incorporates the excluded volume effect resulting from the hard-core repulsion among hadrons.

Here the total excluded volume arising due to  $N$  number of particles having hard core interactions is  $v_0 N$  [50, 51, 56, 57].

The evaluation of the sum over  $N$  in Eq. (7) poses a challenge due to the dependence of the available volume, i.e.,  $V - v_0 N$  on  $N$ . To address this, one can take the Laplace transform on Eq. (7) [51] to get

$$\hat{\mathcal{Z}}_{GC}^{excl}(T, \mu_i, x) = \int_0^\infty dV \exp(-xV) \mathcal{Z}_{GC}^{excl}(T, \mu_i, V) \quad (8)$$

For the finiteness of the above integral and avoid the extreme right singularity in the limit  $V \rightarrow \infty$ , it is required that we should have [51]

$$x = \lim_{V \rightarrow \infty} \frac{\ln \mathcal{Z}_{GC}^{excl}(T, \mu_i, V)}{V} \quad (9)$$

This gives

$$xT = T \lim_{V \rightarrow \infty} \frac{\ln \mathcal{Z}_{GC}^{excl}(T, \mu_i, V)}{V} = p_i^{excl}(T, \mu_i) \quad (10)$$

Using Eq. (7), one can rewrite Eq. (8) as [51]

$$\hat{\mathcal{Z}}_{GC}^{excl}(T, \mu_i, x) = \int_0^\infty dV \exp(-xV) \sum_{N=0}^\infty \exp(\mu_i N/T)$$

$$\times \mathcal{Z}_C^{id}(T, N, V - v_0 N) \quad (11)$$

Interchanging the order of summation and integration, we can therefore rewrite the above Eq. (11) as

$$\hat{\mathcal{Z}}_{GC}^{excl}(T, \mu_i, x) = \sum_{N=0}^\infty \int_0^\infty dV \exp(-xV) \exp(\mu_i N/T) \times \mathcal{Z}_C^{id}(T, N, V - v_0 N) \quad (12)$$

Writing  $V^* = V - v_0 N$  i.e.,  $V = V^* + v_0 N$ , we get

$$\hat{\mathcal{Z}}_{GC}^{excl}(T, \mu_i, V) = \sum_{N=0}^\infty \int_0^\infty dV \exp(-x(V^* + v_0 N)) \times \exp((\mu_i N/T)) \mathcal{Z}_C^{id}(T, N, V^*) \quad (13)$$

As  $N$  is constant in each integral, hence  $dV^* = dV$ , we can rewrite Eq. (13) as

$$\hat{\mathcal{Z}}_{GC}^{excl}(T, \mu_i, V) = \sum_{N=0}^\infty \int_0^\infty dV^* \exp(-xV^*) \times \exp((\mu_i - v_0 T x)(N/T)) \mathcal{Z}_C^{id}(T, N, V^*) \quad (14)$$

Further substituting  $\mu_i^* = \mu_i - v_0 T x$  and again interchanging the order of the integration and summation (replacing the dummy integration variable  $V^*$  by  $V$ )

$$\hat{\mathcal{Z}}_{GC}^{excl}(T, \mu_i, V) = \int_0^\infty dV^* \exp(-xV^*) \sum_{N=0}^\infty \exp(\mu_i^* N/T) \times \mathcal{Z}_C^{id}(T, N, V^*) \quad (15)$$

The above result is as that for the case of point-like particles but with  $\mu_i$  replaced by  $\mu_i^*$ , hence we can finally write

$$\hat{\mathcal{Z}}_{GC}^{excl}(T, \mu_i, V) = \int_0^\infty dV \exp(-xV) \mathcal{Z}_{GC}^{id}(T, \mu_i^*, V) \quad (16)$$

Comparing Eq. (8) and (16), we get

$$\hat{\mathcal{Z}}_{GC}^{excl}(T, \mu_i, V) = \mathcal{Z}_{GC}^{id}(T, \mu_i^*, V) \quad (17)$$

This gives  $p_i^{excl}(T, \mu_i) = p_i^{id}(T, \mu_i^*)$  with  $\mu_i^* = \mu_i - v_0 T x$ . Combining with Eq. (10), it becomes  $\mu_i^* = \mu_i - v_0 p_i^{excl}(T, \mu_i) = \mu_i - v_0 p_i^{id}(T, \mu_i^*)$ . Hence, one can obtain the pressure of the system in the thermodynamic limit  $V \rightarrow \infty$  by solving the transcendental equations.

The number density of the finite size particles can now be obtained in a thermodynamically consistent manner by taking the derivative of the pressure term and after rearranging the terms, we get

$$n_i^{excl}(T, \mu_i) = \left( \frac{\partial p_i^{excl}(T, \mu_i)}{\partial \mu_i} \right)_T = \frac{n_i^{id}(T, \mu_i^*)}{1 + v_0 n_i^{id}(T, \mu_i^*)} \quad (18)$$



Using  $p_i^{excl}(T, \mu_i)$  and  $n_i^{excl}(T, \mu_i)$ , one could derive the  $s_i^{excl}(T, \mu_i)$  and by using the thermodynamical relation  $\varepsilon_i^{excl}(T, \mu_i) = T s_i^{excl}(T, \mu_i) - p_i^{excl}(T, \mu_i) - \mu_i n_i^{excl}(T, \mu_i)$ , we write for the  $i^{th}$  hadronic specie

$$s_i^{excl}(T, \mu_i) = \left( \frac{\partial p_i^{excl}(T, \mu_i)}{\partial T} \right)_T = \frac{s_i^{id}(T, \mu_i^*)}{1 + v_0 n_i^{id}(T, \mu_i^*)} \quad (19)$$

$$\varepsilon_i^{excl}(T, \mu_i) = T s_i^{excl} - p_i^{excl} + \mu_i n_i^{excl} = \frac{\varepsilon_i^{id}(T, \mu_i^*)}{1 + v_0 n_i^{id}(T, \mu_i^*)} \quad (20)$$

where we have used

$$p_i^{excl}(T, \mu_i) = T n_i^{excl}(T, \mu_i) = \frac{T n_i^{id}(T, \mu_i^*)}{1 + v_0 n_i^{id}(T, \mu_i^*)} \quad (21)$$

The above equations reveals two suppression effects because of the VDW repulsion, as

1. The transformation of chemical potential  $\mu_i \rightarrow \mu_i^*$ .
2. A suppression factor  $[1 + v_0 n_i^{id}(T, \mu_i^*)]^{-1} < 1$ .

Eqs. (18), (19), (20) and (21) describe the number density, entropy density, energy density and pressure for a single component of hadronic matter, taking into account finite size effects in a thermodynamically consistent manner. We can generalize this for “ $n$ ” number of hadronic species.

The excluded volume approach can be extended to accommodate several particle species. The excluded volume grand canonical partition function  $\mathcal{Z}_{GC}^{excl}(T, \mu_1, \dots, \mu_n, V)$  for several particle species equals to the product of the partition functions, denoted as  $\mathcal{Z}_{GC}^{excl}(T, \mu_i, V)$  for each individual particle species “ $i$ ” having proper volumes  $v_1, \dots, v_n$  can be defined as

$$\mathcal{Z}_{GC}^{excl}(T, \mu_1, \dots, \mu_n, V) = \sum_{N_1=0}^{\infty} \cdots \sum_{N_n=0}^{\infty} \prod_{i=1}^n \exp\left(\frac{\mu_i N_i}{T}\right) \times \mathcal{Z}_{GC}^{id}(T, N_i, V^*) \theta(V^*) \quad (22)$$

where the available volume is  $V^* = V - \sum_{i=1}^n v_i N_i$ . The Laplace transform of Eq. (22) gives the total pressure

$$p^{excl}(T, \mu_1, \dots, \mu_n) = T \lim_{V \rightarrow \infty} \frac{\ln \mathcal{Z}_{GC}^{excl}(T, \mu_1, \dots, \mu_n, V)}{V} = p^{id}(T, \mu_1^*, \dots, \mu_n^*) = \sum_{i=1}^n p_i^{id}(T, \mu_i^*) \quad (23)$$

The effective baryonic chemical potential  $\mu_i^*$  for  $i^{th}$  baryonic component can then be written as

$$\mu_i^* = \mu_i - v_i p^{excl}(T, \mu_1, \dots, \mu_n) \quad (24)$$

The modified number density of any hadronic species for the multi-component EV-HRG system in the baryonic sector can be obtained in a thermodynamically consistent manner and is thus given as

$$n_i^{excl}(T, \mu_1, \dots, \mu_n) = \left( \frac{\partial p^{excl}}{\partial \mu_i} \right)_{T, \mu_1, \dots, \mu_n} = \frac{n_i^{id}(T, \mu_i^*)}{1 + \sum_{j=1}^n v_j n_j^{id}(T, \mu_j^*)} \quad (25)$$

The effective chemical potential for the  $i^{th}$  antibaryonic component i.e.,  $\bar{\mu}_i^*$  can be obtained in a similar way as given by Eq. (24), by replacing number density of particles  $n_i^{id}$  with antiparticles  $\bar{n}_i^{id}$  and is written as:

$$\bar{\mu}_i^* = \bar{\mu}_i - v_i p^{excl}(T, \bar{\mu}_1, \dots, \bar{\mu}_n); \quad \bar{\mu}_i = -\mu_i \quad (26)$$

The modified number density of the hadronic species for the multi-component EV-HRG system in the antibaryonic sector is thus given as

$$\bar{n}_i^{excl}(T, \bar{\mu}_1, \dots, \bar{\mu}_n) = \left( \frac{\partial \bar{p}^{excl}}{\partial \bar{\mu}_i} \right)_{T, \bar{\mu}_1, \dots, \bar{\mu}_n} = \frac{\bar{n}_i^{id}(T, \bar{\mu}_i^*)}{1 + \sum_{j=1}^n v_j \bar{n}_j^{id}(T, \bar{\mu}_j^*)} \quad (27)$$

In the above, we have presented a comprehensive thermodynamically consistent formulation of the van der Waals (VDW) repulsion within the grand canonical ensemble given by Rischke et. al. [51]. The formulation also addresses a non-trivial problem: the necessity of thermodynamical self-consistency. Other thermal model formulations with ad hoc corrections fall short of this essential condition. Unlike other earlier approaches described in the Ref.'s [32–34, 78], this approach differs significantly in a way that leads to a modified baryon (antibaryon) chemical potential, as shown in Eqs. (24) and (26).

### III. RESULTS AND DISCUSSION

In the preceding sections, we have presented a comprehensive description of the EoS of an EV-HRG, with the main emphasis being on incorporating an essential feature of strong interaction i.e., the hard-core type repulsion among pairs of two baryons or two antibaryons. This effect resembling van der Waals (VDW) type repulsion is incorporated within a grand

canonical ensemble based formulation in a thermodynamically consistent manner. In the present approach, the mesons are treated as point-like particles as they do not exhibit repulsive interaction.

In Eq. (25), the summation over the index  $j$  in the denominator involves all baryonic degrees of freedom, including the  $i^{\text{th}}$  species of baryons (antibaryons). It is noteworthy that the equation of state reflects the influence of repulsive hard-core interactions through the effective baryon chemical potential ( $\mu^*$ ) as given in Eqs. (24) and (26). In order to fix the hard-core volumes of various baryons (antibaryons), we invoke the basic feature of the Bag model, where quarks and gluons are essentially supposed to exist inside a Bag (i.e. hadron), which is assumed to be incompressible [79–81]. The energy density of such a bag is given by  $4B$ , where  $B$  is the bag constant. Using this Bag model approach, the hard-core volume of a baryon with a given mass  $M$  can be written as  $v_0 = M_i/4B$ , where  $M_i$  is the mass of the  $i^{\text{th}}$  hadron [82]. Our best-fitted method to obtain the theoretical fit for the  $\bar{p}/p$  ratio's dependence on  $\sqrt{s_{NN}}$  has yielded  $B = 272 \text{ MeV}/\text{fm}^3$  which provides a very reasonable value of the proton's (antiproton's) hard-core radius of 0.59 fm. This is in agreement with the value obtained by Vovchenko et. al. in [70]. Similarly, for higher mass baryons, it accordingly acquires larger values of hard-core radii (or volumes) by using the same best fitted value of the bag constant. Further, in our approach, we have considered hadrons as incompressible objects but allowed them to get deformed under extreme conditions of temperature and pressure, thus leading to different effective values of the excluded volumes in the system arising due to each baryon (antibaryon). For the case of completely non-deformable spherical baryons (antibaryons), each baryon gives rise to an excluded volume, which is  $4v_0$  while for a fully deformable case, it turns out to be  $v_0$  only. In our present analysis, we have therefore considered a more realistic situation by allowing the baryons and antibaryons to become partly deformable. Hence we have multiplied the baryonic (antibaryonic) hard-core volume  $v_0$  by a deformation factor  $\zeta$  which can vary between 1 and 4. The values 1 and 4 respectively correspond to two extreme ideal situations when baryons (antibaryons) are fully deformable and when they are not deformable at all and are able to retain spherical shape. While using the Eqs. (25) and (27) to describe the relative particle-antiparticle yields, we have therefore treated the quantity  $\zeta$  as a free model parameter along with the other unknown free parameters of the equation. These are fixed by using the best fit method of the experimental data through minimizing the  $\chi^2/\text{dof}$ .

As discussed earlier in Sec. II, the chemical potential  $\mu_i$  of a given  $i^{\text{th}}$  hadronic species is defined in Eq. (2). Since baryons are made up of three valence quarks, the light quark ( $u, d$ ) baryonic chemical potential is defined as  $\mu_q = \mu_B/3$ . The corresponding baryonic fugacity of the light quarks will be  $\lambda_q = e^{\mu_q/T}$  while the light antiquark fugacity will be  $\lambda_{\bar{q}} = \lambda_q^{-1} = e^{-\mu_q/T}$ . Here we have neglected the isospin asymmetry and hence used  $\lambda_u = \lambda_d = \lambda_s$ . This is required to define the fugacities of all the hadrons. In addition, charged hadrons will also acquire electric chemical potential,  $\mu_Q$  in order to control the

net electric charge of the system. The corresponding electric fugacity for a positively charged hadron ( $\pi^+, p, \Sigma^+, \bar{\Sigma}^-$  etc) will be  $\lambda_Q = e^{\mu_Q/T}$ . Similarly for a negatively charged hadron ( $\pi^-, \bar{p}, \bar{\Sigma}^+, \Sigma^-$  etc), we will have  $\lambda_{\bar{Q}} = \lambda_Q^{-1} = e^{-\mu_Q/T}$ , where  $\mu_Q$  is treated as a free parameter and is fixed by conserving the charge-to-baryon ratio of the system. For neutral hadrons,  $\mu_Q = 0$ . The kaon however, contains a light quark (antiquark) and an antistrange (strange) quark therefore, we define kaon fugacities as  $\lambda_{K^+} = \lambda_q \lambda_s^{-1} \lambda_Q$ ,  $\lambda_{K^0} = \lambda_q \lambda_s^{-1}$  etc. The fugacity associated with strange quarks is defined here as  $\lambda_s = e^{\mu_s/T}$ . For strange antiquarks the associated fugacity will be  $\lambda_{\bar{s}} = \lambda_s^{-1} = e^{-\mu_s/T}$ , where  $\mu_s$  is the strange chemical potential and is fixed by applying the criteria of the overall strangeness conservation. As proton and neutron are composed of three light quarks, their fugacities are given as  $\lambda_p = \lambda_q^3 \lambda_Q$  and  $\lambda_n = \lambda_q^3$ . In a similar fashion for the neutral singly strange hyperon ( $\Lambda^0, \Sigma^0$ ) the fugacities becomes  $\lambda_{\Lambda^0, \Sigma^0} = \lambda_q^2 \lambda_s$  and for charged singly strange hyperon ( $\Sigma^+, \Sigma^-$ ) fugacity are defined as  $\lambda_{\Sigma^+} = \lambda_q^2 \lambda_s \lambda_Q$ ,  $\lambda_{\Sigma^-} = \lambda_q^2 \lambda_s \lambda_Q^{-1}$ . For the case of neutral doubly strange hyperon ( $\Xi^0$ ) fugacity will be  $\lambda_{\Xi^0} = \lambda_q \lambda_s^2$  while for the charged doubly strange hyperon i.e., ( $\Xi^-$ ), the fugacity will be  $\lambda_{\Xi^-} = \lambda_q \lambda_s^2 \lambda_Q^{-1}$ . In a similar fashion, we can define the  $\Omega^-$  baryon fugacity as  $\lambda_{\Omega^-} = \lambda_s^3 \lambda_Q^{-1}$ . The chemical potential of all antiparticles is always taken to be the negative of their corresponding particle's chemical potential. Consequently, the fugacities of all antiparticles will be the reciprocal of their corresponding particle's fugacities [17, 57, 58, 81, 83].

There is a strong relationship between these chemical potentials and the temperature of the system i.e.,  $\mu_B, \mu_Q, \mu_S$  and  $T$  inside the hot and dense matter created in the URHIC [84, 85]. As mentioned, in our present approach we have used the net charge to the net baryon number ratio to fix the value of the electric chemical potential,  $\mu_Q$  as

$$\frac{\sum_i n_i(T, \mu_B, \mu_S, \mu_Q, \zeta) Q_i}{\sum_i n_i(T, \mu_B, \mu_S, \mu_Q, \zeta) B_i} = \text{constant} \quad (28)$$

The summation in the numerator is over all charged particle densities, where  $Q_i = +1(+2)$  and  $-1(-2)$  respectively for positive singly (doubly) and negative singly (doubly) charged particle. In the denominator the summation is over all baryon and antibaryon densities where  $B_i = +1$  for baryons and  $-1$  for antibaryons. The physical systems formed in the ultra-relativistic nucleus-nucleus collisions determine the ratio of the net charge to the net baryon number. It is seen that the ratio of the number of protons ( $N_p$ ) to the mass number ( $N_p + N_n$ ) of the colliding nuclei in the URHIC experiments is nearly constant, i.e.,  $\sim 0.4$ .

The strange chemical potential  $\mu_S(T, \mu_B, \mu_Q, \zeta)$  of the system is determined by the overall *net zero* strangeness

$$n_S(T, \mu_B, \mu_S, \mu_Q, \zeta) = \sum_i s_i n_i(T, \mu_B, \mu_S, \mu_Q, \zeta) - \sum_i \bar{s}_i \bar{n}_i(T, \mu_B, \mu_S, \mu_Q, \zeta) = 0 \quad (29)$$

In the above equation, the  $s_i$  and  $n_i$  are the strangeness content and number density of the  $i^{th}$  strange hadron. Similarly, the  $\bar{s}_i$  and  $\bar{n}_i$  are for the cases of the corresponding antiparticles.

Now the two remaining thermodynamic parameters, i.e., temperature ( $T$ ) and baryon chemical potential ( $\mu_B$ ) at various collision energies can be fixed by fitting the experimental data on antibaryon to baryon ratios available over a wide range of collision energy ( $\sqrt{s_{NN}}$ ). As already discussed the baryon chemical potential reflects the excess of baryons over antibaryons. On the other hand, an increasing temperature leads to significant excitation within the system, causing the densities of all particles to increase and hence strongly affecting the particle ratios.

Hence,  $T$  and  $\mu_B$  of the systems formed in the URHIC at different collision energies ( $\sqrt{s_{NN}}$ ) at chemical freeze-out must be precisely determined in order to perform a useful comparison between theoretical and experimental data. An effective way to achieve this goal is to create a relationship between these two freeze-out parameters and  $\sqrt{s_{NN}}$ . The following type of ansatz has been widely used in the literature to fit the extracted values of  $T$  and  $\mu_B$  from the experimental data [86–92].

$$\mu_B = \frac{a}{1 + b\sqrt{s_{NN}}} \quad (30)$$

$$T = c - d\mu_B^2 - e\mu_B^4 \quad (31)$$

This kind of ansatz has shown promising results in examining the characteristics of hot and dense matter in URHIC using thermal models across various colliding energies. Analysis over a broad collision energy range [16, 21, 93] have contributed significantly in advancing our comprehension of the criteria governing thermo-chemical freeze-out.

It is customary to include all baryonic and mesonic resonances in the system and the contribution of their subsequent decays to the observed final state hadrons in the experiments. It is also important to note that the final number density of hadronic species is modified due to the feed-down decay contribution of the heavier resonances. We have included hadronic resonances upto 2 GeV mass [94–96]. The final state particle multiplicities are then represented by the following

$$n_i^f = n_i^{excl} + \sum_j \Gamma_{j \rightarrow i} n_j^{excl} \quad (32)$$

$$\bar{n}_i^f = \bar{n}_i^{excl} + \sum_j \Gamma_{j \rightarrow i} \bar{n}_j^{excl} \quad (33)$$

where  $n_i^{excl}$  is the thermal particle number density which is calculated using Eq. (25) and  $\bar{n}_i^{excl}$  is the thermal antiparticle number density, which is calculated using Eq. (27). In the above equations,  $\Gamma_{j \rightarrow i}$  is the probability of particle  $j$  decay into particle  $i$  [96].

In our present analysis, the values of the constants in the above Eqs. (30) and (31) are obtained by the least  $\chi^2$  fitting procedure of  $\bar{p}/p$  ratios available over a wide range of collision energy. The  $\chi^2$  is defined as

$$\chi^2 = \sum_{i=1}^h \left( \frac{R_i^{theo} - R_i^{expt}}{\sigma_i} \right)^2 \quad (34)$$

The  $R_i^{theo}$  and  $R_i^{expt}$  are the theoretical results and experimental values of the particle ratios for  $i^{th}$  collision energy  $\sqrt{s_{NN}}$  and  $\sigma_i$  represent the experimental (statistical systematic) errors for corresponding energies. The values obtained are  $a = 1310.0$  MeV,  $b = 0.31$  GeV $^{-1}$ ,  $c = 166.0$  MeV,  $d = 0.33 \times 10^{-3}$  MeV $^{-1}$ ,  $e = 0.015 \times 10^{-9}$  MeV $^{-3}$  and  $\zeta = 2.8$ . The number of data points for the case of the  $\bar{p}/p$  ratio in the experimental data set [97–102] is 18, as shown in Fig. 1.

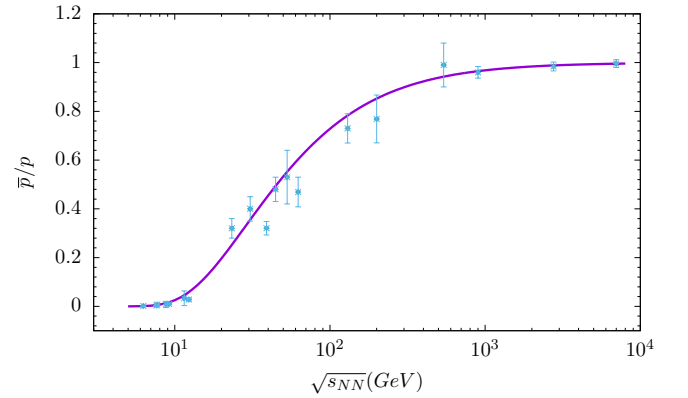


FIG. 1.  $\bar{p}/p$  dependence on  $\sqrt{s_{NN}}$ . Experimental data is taken from [97–102].

Using these extracted values of the system parameters, we first show the variation of temperature ( $T$ ) and BCP ( $\mu_B$ ) of the baryons in the system with the centre of mass collision energy  $\sqrt{s_{NN}}$ , in Fig. 2, represented by Eqs. (30) and (31), respectively. The extracted values of  $\mu_B$  falls monotonically from SIS and AGS energy range to Relativistic Heavy-Ion Collider (RHIC) at BNL and further towards the LHC energies while extracted temperature  $T$  is seen to rise asymptotically almost saturating at 166 MeV for baryons (antibaryons). In other words, the central collisions at higher energies can be characterized by a unique (almost) energy independent chemical freeze-out temperature. This baryonic freeze-out temperature value is in close proximity to the phase-transition temperature predicted by the lattice QCD calculations. This indicates that in very high energy nuclear collisions, the system undergoes a chemical decoupling close to the phase boundary.

The proton (antiproton) is the lightest baryon (antibaryon). As most of the high-mass baryons (antibaryons) decay into protons (antiprotons), it is worthwhile to note that protons and antiprotons are of particular importance because of their large abundance in the final state among all baryons in URHIC. Hence, we have used their abundances to extract the  $T$  and

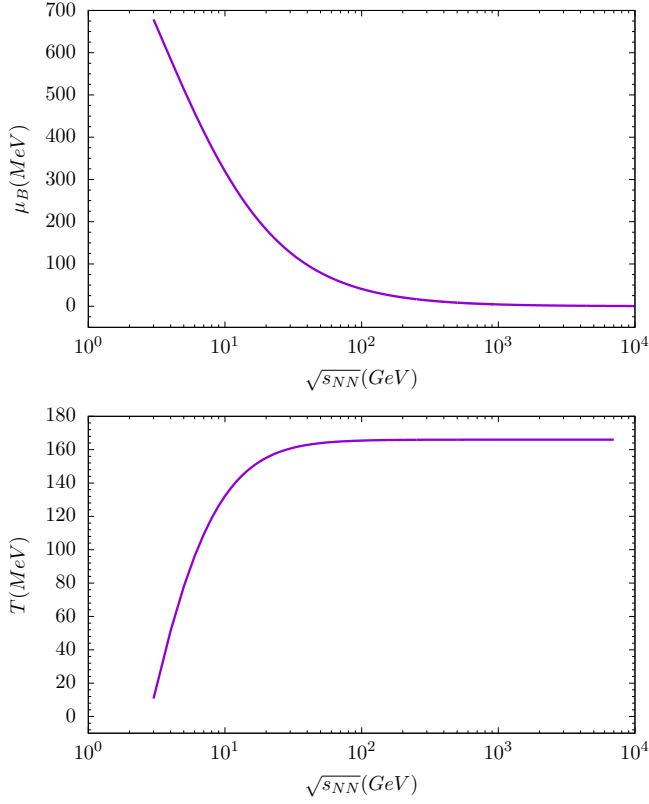


FIG. 2. Dependence of BCP ( $\mu_B$ ) and temperature ( $T$ ) on  $\sqrt{s_{NN}}$  for baryonic degrees of freedom

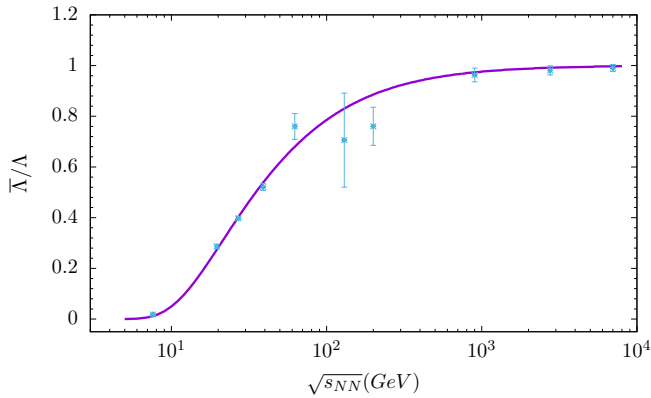


FIG. 3.  $\bar{\Lambda}/\Lambda$  dependence on  $\sqrt{s_{NN}}$ . Experimental data is taken from [99, 101, 103–105]

BCP values of the system for all baryonic (antibaryonic) degrees of freedom. Here the inclusive yield of protons (as well as all other hadrons) is reported as the sum of their primordial yields and the decay contributions after the chemical freeze-out. We have taken into account the contributions of single weak decay processes and where a weak decay is followed by a strong decay. The final state hadron multiplicities can only be understood in a better way by taking these decay modes

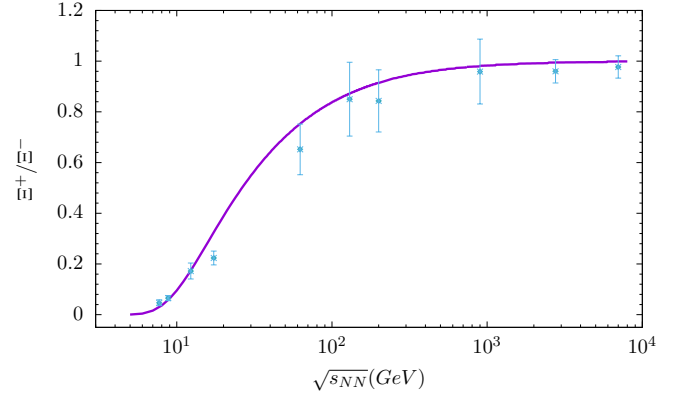


FIG. 4.  $\Xi^+/\Xi^-$  dependence on  $\sqrt{s_{NN}}$ . Experimental data is taken from [99, 101, 103–105]

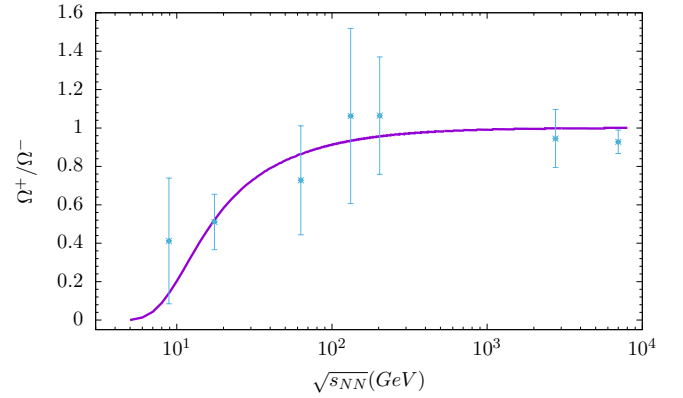


FIG. 5.  $\Omega^+/\Omega^-$  dependence on  $\sqrt{s_{NN}}$ . Experimental data is taken from [99, 101, 103–105]

into account [106].

The decreasing value of  $\bar{p}/p$  towards lower  $\sqrt{s_{NN}}$  reflects an increase in the net baryon density due to higher baryon stopping at lower collision energies, as seen in Fig. 1. The antiproton yield however increases with increasing collision energies more rapidly than the proton. Towards sufficiently higher values of  $\sqrt{s_{NN}}$ , the production of protons and antiprotons becomes almost equal due to increasing temperature, as there is relatively more thermal production of antiprotons at higher temperatures. Further, due to the increasing transparency effect in nuclear collisions at higher energies, the bulk of the secondary hadronic matter is formed between the two receding nuclei. Consequently, the system tends to become symmetric between baryons and antibaryons and hence maintains a small baryon chemical potential as there is very little excess of baryons over antibaryons.

Similarly, other antibaryon to baryon ratios, like  $\bar{\Lambda}/\Lambda$ ,  $\Xi^+/\Xi^-$  and  $\Omega^+/\Omega^-$  are shown in Figs. 3, 4, 5, respectively. We have chosen the same set of freeze-out parameters for these cases, as obtained from the best-fit curve for the  $\bar{p}/p$  ratio, thus assuming simultaneous freeze-out of all baryonic



species in the system [70]. These ratios also show an increasing trend with increasing collision energy. Beyond  $\sqrt{s_{NN}} \sim 200$  GeV, the ratios tend to saturate towards unity, exhibiting clear evidence of nearly equal production of baryons and antibaryons in the URHIC. In all the above cases, we find that the theoretically fitted curves are in good agreement with the trend exhibited by the experimental data. The minimum  $\chi^2/\text{dof}$  for the best fitted curve in the case of the  $\bar{p}/p$  ratio is 1.56 where dof in this case is 18. While for the cases of  $\bar{\Lambda}/\Lambda$ ,  $\Xi^+/\Xi^-$ ,  $\Omega^+/\Omega^-$ , it turns out to be 1.23, 1.90 and 0.40 using the same set of parameters as already discussed above.

One important observation in our study is that a lower chemical freeze-out temperature than that of baryons is required to explain the  $\sqrt{s_{NN}}$  dependence of the  $K^-/K^+$  ratio as well as the charged pion ratio, i.e.,  $\pi^-/\pi^+$ .

We find clear evidence that the baryons have a higher chemical freeze-out temperature than that of mesons. In earlier studies, two different freeze-out temperatures for baryon and meson sectors in thermal models have been discussed in relation to Hagedorn's states [107, 108]. The best-fit curve shows the  $K^-/K^+$  dependence on  $\sqrt{s_{NN}}$  which is obtained only by using a lower value of the temperature ansatz parameter, i.e.,  $c = 152$  MeV in Eq. (31) while for baryons it is 166 MeV. The values of the remaining parameters remain unchanged.

We find that the  $K^-/K^+$  ratio increases with increasing collision energy,  $\sqrt{s_{NN}}$  and then saturates as it approaches unity beyond  $\sqrt{s_{NN}} \sim 200$  GeV. This may be attributed to almost symmetric particle and antiparticle production at high energies, as shown in Fig. 6

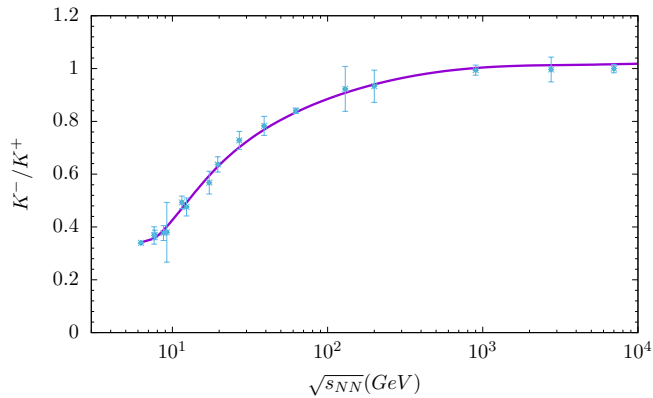
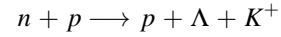
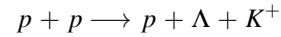
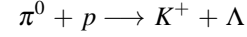
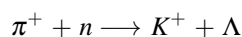


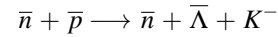
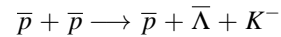
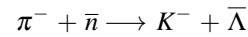
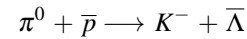
FIG. 6.  $K^-/K^+$  dependence on  $\sqrt{s_{NN}}$ . Experimental data is taken from [100, 103, 109]

The increase in the  $K^-/K^+$  ratio with  $\sqrt{s_{NN}}$  indicates that the production channels of  $K^+$  and  $K^-$  contribute almost equally to their abundances as the matter becomes baryon symmetric. Consequently, baryons and antibaryons contribute to the abundance of  $K^+$  and  $K^-$  almost equally. However, at lower energies, the production of  $K^+$  dominates due to an excess of baryons over antibaryons.

The reactions for the production of  $K^+$  involving the above-mentioned interactions are mainly:



While the reactions for the production of  $K^-$  (involving antinucleons) are mainly:



The  $\pi\pi \longrightarrow K^+K^-$  reaction channel however produces  $K^-$  and  $K^+$  in a symmetric manner. As illustrated above, at lower collision energies, there is more production of  $K^+$  in the system due to the dominance of baryons over antibaryons states. Our thermal model-based predictions are in accordance with this scenario. The experimental data on  $K^-$  and  $K^+$  abundance ratios closely matches the predictions of the thermal model. This agreement strengthens our notion of that thermal models may adequately represent the dynamics of particle production at different collision energies.

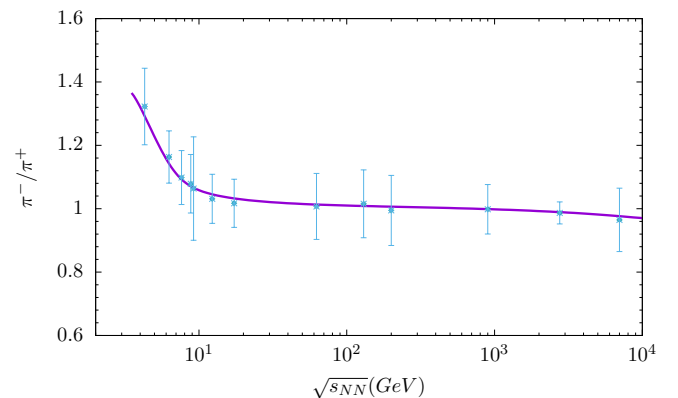


FIG. 7.  $\pi^-/\pi^+$  dependence on  $\sqrt{s_{NN}}$ . Experimental data is taken from [97, 103]

Charged hadrons are produced at different stages in the system formed in URHIC during its evolution [110–112]. Pion is

the lightest among all charged hadrons and is thus abundantly produced during the evolution of the system until freeze-out and carries only electric charge (i.e. neither strangeness nor baryon number). The thermal production ratio  $\pi^-/\pi^+$  is, however, not only governed by the electric chemical potential, i.e.,  $\mu_Q$ , but also by the chemical freeze-out temperature  $T$ . Besides, several heavier hadronic resonances, including baryons and kaons, contribute to its final stage abundance through their various decay channels. Hence, the ratio  $\pi^-/\pi^+$ , besides  $\mu_Q$  and  $T$ , also exhibits its dependence on baryon chemical potential  $\mu_B$ .

At low energies, the secondary heavier resonances are much less produced and the positive charged are mostly trapped inside the protons. Hence any extra positive charge of the secondary hadrons is compensated by the production of  $\pi^-$ . This causes an increase in the  $\pi^-$  production as compared to the  $\pi^+$  production. However, at sufficiently higher energies, there is almost symmetric production of positive and negative pions in the system as the system maintains an overall low net baryon density (i.e., small  $\mu_B$ ). The ratio thus tends to saturate to unity for the energies beyond  $\sqrt{s_{NN}} \sim 10$  GeV, as shown in Fig. 7.

Kaon is the most abundantly produced strange hadron in heavy-ion collisions as it is the lightest strange particle having mass much less than the lightest baryon i.e., proton ( $m_K \ll m_p$ ). The strangeness (antistrangeness) content of the system is thus mostly carried by the kaons. Similarly, as discussed above, pions ( $\pi$ ) being the most abundantly produced particles in URHIC carry bulk of the entropy content of the system. The  $K/\pi$  ratio is therefore of particular interest, as it reflects the strangeness content relative to the entropy content of the system formed in ultra-relativistic heavy-ion collisions. This ratio is also an indicator of the enhanced strangeness production in the highly excited thermalized system formed in the URHIC [113–115]. Initially, it was suggested that the enhanced  $K/\pi$  ratio could potentially serve as a possible signature of QGP [116] formation, but their precise connection to the properties of phase transition remains skeptical [117]. Therefore, there still remains an ambiguity as to how  $K/\pi$  could be regarded an unambiguous indicator of the transition between QGP and hadronic matter in heavy-ion collisions. It is also been suggested that a chemically equilibrated hadronic resonance gas (HRG) might exhibit strangeness comparable to or greater than that of QGP [43, 118–120]. The present calculations clearly show that in order to explain all strange (antistrange) to non-strange hadronic ratios obtained within the framework of thermal hadron resonance gas (HRG) model require a “strangeness (antistrangeness) imbalance factor”,  $\gamma_s$ . Above  $\sqrt{s_{NN}} \sim 10$  GeV, the factor turns out to be less than unity ( $\gamma_s < 1$ ) indicating a suppression in the  $K^-/\pi^-$  yield in the experiments. While below this energy, there is evidence of excess experimental yield compared to the theoretically obtained values, thus providing  $\gamma_s > 1$ . This phenomenon may be interpreted as evidence of a non-equilibrium effect in the production of strangeness [44, 45]. It has also been suggested that an observably low  $K^-/\pi^-$  yield above  $\sqrt{s_{NN}} \sim 10$  GeV may be a signature of QGP presence followed by a non-equilibrium effect during the QGP to HRG

transition, especially in the kaonic sector [121, 122]. While at lower energies, where the experimental  $K^-/\pi^-$  ratios are greater than the theoretical ones, it can be safely assumed that no QGP is formed and the system remains in the HRG phase. In such a system, a certain fraction of pions may get absorbed through the strangeness producing reactions ( $\pi\pi \rightarrow K\bar{K}$ ,  $\pi N \rightarrow K\Lambda$ ,  $\pi\bar{N} \rightarrow \bar{K}\Lambda$ ), while due to possible non-equilibrium effects, the backward reaction rates remain slower than the forward ones, leading to a depletion of pions and increase in the kaon population, consequently leading to an enhanced  $K^-/\pi^-$  ratio. Thus, this ratio in URHIC may offer a more insightful perspective, especially when compared to proton-proton collisions [40, 87, 123]. The present work thus also attempts to study the  $K/\pi$  ratio and the effect of strangeness imbalance over a wide range of collision energy by taking into account the hard-core hadronic repulsion’s. We find that near  $\sqrt{s_{NN}} = 10$  GeV, our theoretical value of the  $K^-/\pi^-$  ratio is  $\sim 0.1$ , which matches quite well with experimental data. Hence, in this case, the strangeness imbalance factor  $\gamma_s$  turn out to be  $\sim 1$ . This may be due to the competing effect of a predominantly HRG type system and the beginning of the onset of deconfinement.

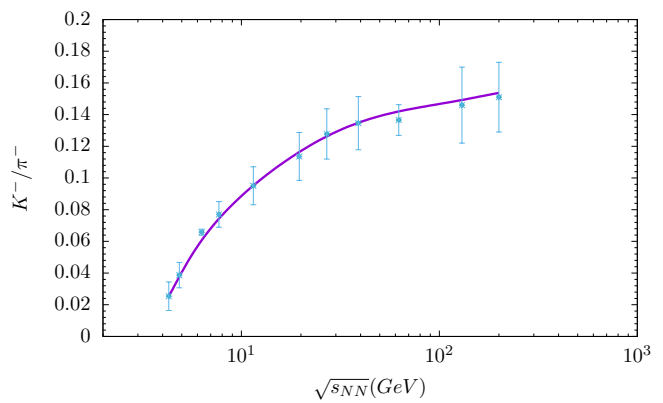


FIG. 8.  $K^-/\pi^-$  dependence on  $\sqrt{s_{NN}}$ . Experimental data is taken from [100, 103, 104, 109]

In Fig. 8, we have shown a variation of the corrected  $K^-/\pi^-$  ratio with  $\sqrt{s_{NN}}$ , wherein we have multiplied the theoretically obtained values with the strangeness imbalance factor  $\gamma_s$ . This provides  $\chi^2/\text{dof}$  to be 0.23 for  $K^-/\pi^-$  ratio. The ratio increases steadily with increasing  $\sqrt{s_{NN}}$  up to  $\sim 50$  GeV in the URHIC and saturates towards further higher energies at  $\sim 0.16$ .

It is very interesting to note here that the values of the strangeness imbalance factor obtained from the analysis of the  $K^-/\pi^-$  ratio can be used to obtain reasonably correct values of the  $K^+/\pi^+$  ratio over a wide range of collision energy. The resulting (corrected) theoretical values are found to fit the experimental data quite well, including the region of energy (5–7) GeV [124, 125], where a horn structure is seen in Fig. 9.

For a nearly baryon symmetric matter formed in URHIC having  $\mu_B \sim 0$ , the  $K^-/\pi^-$  and  $K^+/\pi^+$  would become nearly

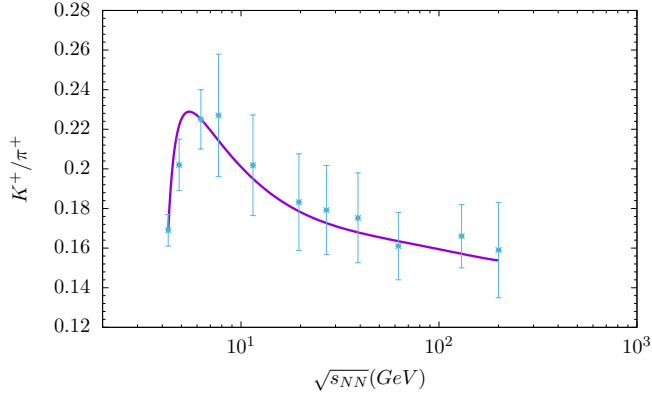


FIG. 9.  $K^+/\pi^+$  dependence on  $\sqrt{s_{NN}}$ . Experimental data is taken from [100, 103, 104, 109]

identical. This is clearly seen in the two Figs. 8 and 9 where both ratios tend to saturate at  $\sim 0.16$  for large values of  $\sqrt{s_{NN}}$ . The existence of the ‘‘horn’’ structure in the  $K^+/\pi^+$  ratio may be explained in terms of higher kaon production rates compared to that of the antikaons [126, 127] as already discussed above. Here it is worthwhile to mention that the previously shown antihyperon to hyperon ratios in Figs. 3, 4 and 5 are almost independent of  $\gamma_s$  as their strangeness-antistrangeness contents are equal and are hence equally affected by this factor.

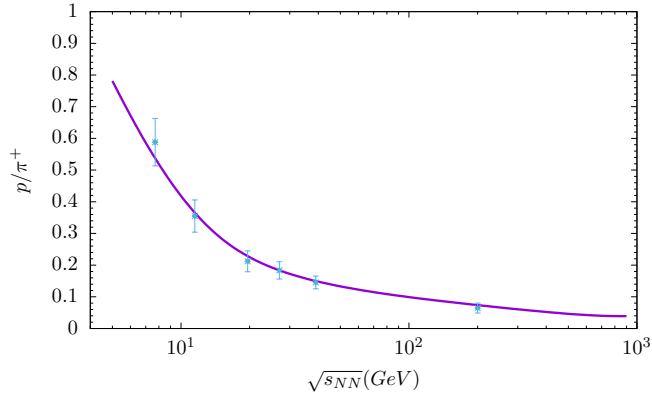


FIG. 10.  $p/\pi^+$  dependence on  $\sqrt{s_{NN}}$ . Experimental data is taken from [97, 99, 103]

In Figs. 10 and 11, we have shown the dependence of  $p/\pi^+$  and  $\bar{p}/\pi^-$  ratios on  $\sqrt{s_{NN}}$ . These ratios serve as indicators of the relative yields of the lightest baryons (antibaryons) and mesons. The apparently good agreement between the theoretical and experimental value can characterize the thermal nature of the hadron production with in hot and dense fireball consisting of various hadronic resonances. In Fig. 10, the value of  $p/\pi^+$  ratio decreases monotonically. This could be due to the fact that at lower collision energies the baryon chemical potential of the system is high ( $\sim 500$  MeV) which

tends to enhance the baryon abundance while suppressing the antibaryon abundance. Hence at lower  $\sqrt{s_{NN}}$  we have a proton rich system. However, with increasing collision energy the temperature of the HRG system formed in URHIC increases (asymptotically) but the baryon chemical potential simultaneously decreases. This results in a relatively slower increase in the fermionic, i.e., protonic, abundance than that of the light bosonic i.e., pionic abundance in the system thus leading to a decrease in the  $p/\pi^+$  ratio with increasing  $\sqrt{s_{NN}}$ .

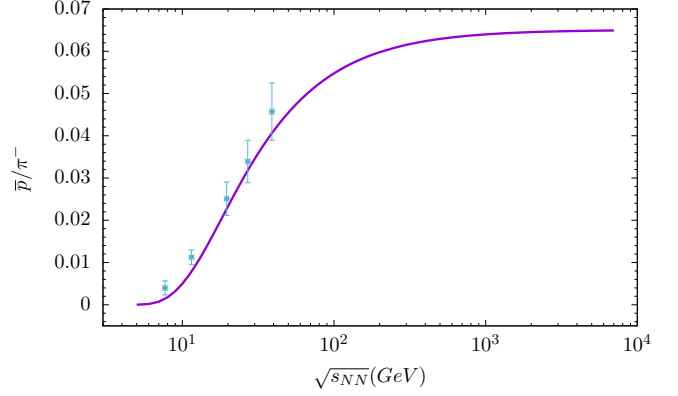


FIG. 11.  $\bar{p}/\pi^-$  dependence on  $\sqrt{s_{NN}}$ . Experimental data is taken from [97, 99, 103]

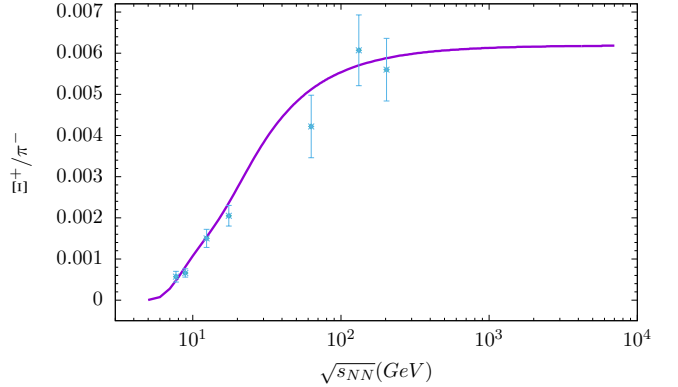


FIG. 12.  $\Xi^+/\pi^-$  dependence on  $\sqrt{s_{NN}}$ . Experimental data is taken from [97, 99, 103, 104]

Since towards higher collision energies the decreasing baryon chemical potential and the rising temperature leads to a rapid increase in the antiproton abundance than that of the proton hence the ratio  $\bar{p}/\pi^-$  is seen to rise with  $\sqrt{s_{NN}}$  in Fig. 11. Similarly the cascade antibaryon to pion ratio i.e.,  $\Xi^+/\pi^-$  is also seen to increase in Fig. 12 with the center-of-mass energy  $\sqrt{s_{NN}}$ . The theoretical curve obtained after applying the strangeness imbalance correction factor  $\gamma_s$  is found to explain the available experimental data well with  $\chi^2/\text{dof}$  equals to 0.85.

#### IV. SUMMARY AND CONCLUSION

An improved thermodynamically consistent hadron resonance gas (HRG) model is used in this study by taking excluded volume (EV) effects into consideration in order to explain several relative hadronic yields in URHIC over a wide range of collision  $\sqrt{s_{NN}}$  energy using a set of model parameters. We have assigned a hard-core finite size volume to baryons (antibaryons) through bag model approach using  $B=272$  MeV/fm<sup>3</sup>. For protons, this gives a radius of 0.59 fm which is a reasonable value. The hard-core volumes of the other baryons (antibaryons) increase according to their masses. The mesons have been treated as point particles. We find that though the baryons and antibaryons may be treated as incompressible however they appear to be partly deformable, where the deformation factor  $\zeta$  is  $\sim 2.8$ . Our approach remains quiet valid even at values of thermodynamic variables, i.e., temperature ( $T$ ) and baryon chemical potential ( $\mu_B$ ) of the HRG system under extreme conditions. The centre-of-mass energy  $\sqrt{s_{NN}}$  dependent ansatz is used for fixing the values of these two thermodynamic variables ( $T$ ) and ( $\mu_B$ ). Clear evidence of a double chemical freeze-out scenario, one cor-

responding to baryons (antibaryons) and the other to mesons, is seen. The baryons are found to freeze-out earlier than the mesons. We also take into account the final state contributions of the heavier hadronic resonances with masses up to 2 GeV through their weak decays. We have included single weak decays as well as the double decays where weak decay is followed by strong decay. We use minimum  $\chi^2/\text{dof}$  fits to theoretically explain the variation of the experimental particle ratios with centre-of-mass collision energy. When attempting to explain the unlike mass ratios of strange and non-strange hadrons, e.g.,  $K/\pi$  and  $\Xi^+/\pi^-$ , we find that the theoretical results overestimate the experimental data significantly. In order to achieve a reasonably good agreement between the theoretical results with the experimental data, we have introduced a strangeness (anti)strangeness imbalance factor,  $\gamma_s$ , which can explain the abundance of strange hadrons relative to non-strange ones, especially pions, which are the most abundantly produced non-strange hadrons. After applying the same strangeness imbalance correction factor  $\gamma_s$  to each case, we find that the theoretical curves match quite well with the trend of the experimental data, with reasonable values of the minimum  $\chi^2/\text{dof}$  for each case.

- 
- [1] F. Wilczek, *Rev. Mod. Phys.* **71**, S85 (1999).
- [2] N. Cabibbo and G. Parisi, *Phys. Lett. B* **59**, 67 (1975).
- [3] E. V. Shuryak, *Sov. Phys. JETP* **47**, 212 (1978).
- [4] A. Bazavov, T. Bhattacharya, C. DeTar, H.-T. Ding, S. Gottlieb, R. Gupta, P. Hegde, U. M. Heller, F. Karsch, E. Laermann, L. Levkova, S. Mukherjee, P. Petreczky, C. Schmidt, C. Schroeder, R. A. Soltz, W. Soeldner, R. Sugar, M. Wagner, and P. Vranas (HotQCD Collaboration), *Phys. Rev. D* **90**, 094503 (2014).
- [5] A. Collaboration, The alice experiment : A journey through qcd (2022), [arXiv:2211.04384 \[nucl-ex\]](https://arxiv.org/abs/2211.04384).
- [6] A. Collaboration, Multiplicity dependence of charged-particle intra-jet properties in pp collisions at  $\sqrt{s} = 13$  tev (2023), [arXiv:2311.13322 \[hep-ex\]](https://arxiv.org/abs/2311.13322).
- [7] B. Müller, *Nuclear Physics A* **544**, 95 (1992).
- [8] S. A. Bass and A. Dumitru, *Phys. Rev. C* **61**, 064909 (2000).
- [9] A. Mekjian, *Phys. Rev. Lett.* **38**, 640 (1977).
- [10] J. Gosset, J. I. Kapusta, and G. D. Westfall, *Phys. Rev. C* **18**, 844 (1978).
- [11] A. Z. Mekjian, *Nucl. Phys. A* **312**, 491 (1978).
- [12] L. Csernai and J. I. Kapusta, *Physics Reports* **131**, 223 (1986).
- [13] D. Hahn and H. Stöcker, *Phys. Rev. C* **35**, 1311 (1987).
- [14] D. Hahn and H. Stöcker, *Nucl. Phys. A* **476**, 718 (1988).
- [15] P. Braun-Munzinger and J. Stachel, *Nucl. Phys. A* **606**, 320 (1996).
- [16] F. Becattini, J. Cleymans, A. Keränen, E. Suhonen, and K. Redlich, *Phys. Rev. C* **64**, 024901 (2001).
- [17] S. Uddin, *Eur. Phys. J. C* **6**, 355 (1998).
- [18] U. W. Heinz, (2004), [arXiv:hep-ph/0407360 \[hep-ph\]](https://arxiv.org/abs/hep-ph/0407360).
- [19] R. A. Bhat, S. Uddin, and I. ul Bashir, *Nucl. Phys. A* **935**, 43 (2015).
- [20] J. Cleymans, B. Kämpfer, M. Kaneta, S. Wheaton, and N. Xu, *Phys. Rev. C* **71**, 054901 (2005).
- [21] J. Letessier and J. Rafelski, *Eur. Phys. J. A* **35**, 221 (2008).
- [22] F. Becattini, An introduction to the statistical hadronization model (2009), [arXiv:0901.3643 \[hep-ph\]](https://arxiv.org/abs/0901.3643).
- [23] A. Andronic, P. Braun-Munzinger, K. Redlich, and J. Stachel, *Nature* **561**, 321 (2018).
- [24] S. Borsányi, Z. Fodor, S. Katz, S. Krieg, C. Ratti, and K. Szabó, *J. High Energy Phys.* **2012**, 138.
- [25] A. Bazavov, T. Bhattacharya, C. E. DeTar, H.-T. Ding, S. Gottlieb, R. Gupta, P. Hegde, U. M. Heller, F. Karsch, E. Laermann, L. Levkova, S. Mukherjee, P. Petreczky, C. Schmidt, R. A. Soltz, W. Soeldner, R. Sugar, and P. M. Vranas (HotQCD Collaboration), *Phys. Rev. D* **86**, 034509 (2012).
- [26] R. Bellwied, S. Borsányi, Z. Fodor, S. D. Katz, A. Pásztor, C. Ratti, and K. K. Szabó, *Phys. Rev. D* **92**, 114505 (2015).
- [27] R. Bellwied, S. Borsanyi, Z. Fodor, S. D. Katz, and C. Ratti, *Phys. Rev. Lett.* **111**, 202302 (2013).
- [28] D. Rischke, M. Gorenstein, H. Stöcker, and W. Greiner, *Z. Phys. C* **51**, 485 (1991).
- [29] G. D. Yen, M. I. Gorenstein, W. Greiner, and S. N. Yang, *Phys. Rev. C* **56**, 2210 (1997).
- [30] G. D. Yen and M. I. Gorenstein, *Phys. Rev. C* **59**, 2788 (1999).
- [31] L. M. Satarov, V. Vovchenko, P. Alba, M. I. Gorenstein, and H. Stoecker, *Phys. Rev. C* **95**, 024902 (2017).
- [32] J. Cleymans and H. Satz, *Z. Phys. C* **57**, 135 (1993).
- [33] J. Cleymans, K. Redlich, H. Satz, and E. Suhonen, *Z. Phys. C* **58**, 347 (1993).
- [34] P. Braun-Munzinger, J. Stachel, J. P. Wessels, and N. Xu, *Phys. Lett. B* **344**, 43 (1995).
- [35] P. Braun-Munzinger, J. Stachel, J. Wessels, and N. Xu, *Physics Letters B* **365**, 1 (1996).
- [36] R. A. Ritchie, M. I. Gorenstein, and H. G. Miller, *Z. Phys. C* **75**, 535 (2014).
- [37] V. Vovchenko, D. V. Anchishkin, and M. I. Gorenstein, *Phys. Rev. C* **91**, 064314 (2015).
- [38] V. Vovchenko, M. I. Gorenstein, and H. Stoecker, *Phys. Rev. Lett.* **118**, 182301 (2017).



- [39] V. Vovchenko, A. Motornenko, P. Alba, M. I. Gorenstein, L. M. Satarov, and H. Stoecker, *Phys. Rev. C* **96**, 045202 (2017).
- [40] V. K. Tiwari and C. P. Singh, *Phys. Lett. B* **421**, 363 (1998).
- [41] S. Pratt and C. Plumberg, *Phys. Rev. C* **104**, 014906 (2021).
- [42] P. Koch, B. Muller, and J. Rafelski, *Physics Reports* **142**, 167 (1996).
- [43] G. Baym, *Nucl. Phys. A* **479**, 27 (1988).
- [44] M. Gaździcki, *APH N.S. Heavy Ion Physics* **4**, 33 (1996).
- [45] M. Gaździcki, *J. Phys. G: Nucl. Part. Phys.* **23**, 12 (1881).
- [46] C. P. Singh, P. K. Srivastava, and S. K. Tiwari, *Phys. Rev. D* **83**, 039904 (2011).
- [47] J. Cleymans and E. Suhonen, *Z. Phys. C* **37**, 51 (1987).
- [48] R. Hagedorn and J. Rafelski, *Physics Letters B* **97**, 136 (1980).
- [49] R. Hagedorn, *Z. Phys. C* **17**, 265 (1983).
- [50] H. Kuono and F. Takagi, *Z. Phys. C* **42**, 209 (1989).
- [51] D. Rischke, M. Gorenstein, H. Stöcker, and W. Greiner, *Z. Phys. C* **51**, 485 (1991).
- [52] J. I. Kapusta, *Phys. Rev. D* **23**, 2444 (1981).
- [53] J. I. Kapusta and K. A. Olive, *Phys. Lett. B* **209**, 295 (1988).
- [54] Q. R. Zhang, *Z. Phys. C* **351**, 89 (1995).
- [55] B.-Q. Ma, Q.-R. Zhang, D. Rischke, and W. Greiner, *Physics Letters B* **315**, 29 (1993).
- [56] S. Uddin and C. P. Singh, *Z. Phys. C* **63**, 147 (1993).
- [57] S. Uddin, *Phys. Lett. B* **341**, 361 (1995).
- [58] S. A. Mir, N. A. Rather, I. M. U. Din, and S. Uddin, (2024), [arXiv:2312.13079 \[hep-ph\]](https://arxiv.org/abs/2312.13079).
- [59] K. Bugaev, M. Gorenstein, H. Stöcker, and W. Greiner, *Physics Letters B* **485**, 121 (2000).
- [60] S. K. Tiwari, P. K. Srivastava, and C. P. Singh, *Phys. Rev. C* **85**, 014908 (2012).
- [61] I. G. Bearden *et al.* (BRAHMS Collaboration), *Phys. Rev. Lett.* **93**, 102301 (2004).
- [62] J. Cleymans, J. Strümpfer, and L. Turko, *Phys. Rev. C* **78**, 017901 (2008).
- [63] A. Buzzatti and M. Gyulassy, *Nuclear Physics A* **904-905**, 779c (2013), the Quark Matter 2012.
- [64] A. Andronic, P. Braun-Munzinger, and J. Stachel, *Nucl. Phys. A* **772**, 167 (2006).
- [65] S. Wheaton, J. Cleymans, and M. Hauer, *Computer Physics Communications* **180**, 84 (2009).
- [66] V. Vovchenko and H. Stoecker, *Computer Physics Communications* **244**, 295 (2019).
- [67] A. Kisiel, T. Tałuć, W. Broniowski, and W. Florkowski, *Computer Physics Communications* **174**, 669 (2006).
- [68] M. Gorenstein, V. Petrov, and G. Zinovjev, *Physics Letters B* **106**, 327 (1981).
- [69] R. Hagedorn and J. Rafelski, *Phys. Lett. B* **97**, 136 (1980).
- [70] V. Vovchenko, M. I. Gorenstein, and H. Stoecker, *Phys. Rev. Lett.* **118**, 182301 (2017).
- [71] V. Vovchenko, D. V. Anchishkin, and M. I. Gorenstein, *Phys. Rev. C* **91**, 064314 (2015).
- [72] V. Vovchenko, D. Anchishkin, M. I. Gorenstein, and R. V. Poberezhnyuk, *Phys. Rev. C* **92**, 054901 (2015).
- [73] S. Samanta and B. Mohanty, *Phys. Rev. C* **97**, 015201 (2018).
- [74] A. Andronic, P. Braun-Munzinger, J. Stachel, and M. Winn, *Phys. Lett. B* **718**, 80 (2012).
- [75] D. Granddon, M. I. Gorenstein, W. Greiner, and S. Nan Yang, *Phys. Rev. C* **56**, 2210 (1997).
- [76] K. K. Pradhan, D. Sahu, R. Scaria, and R. Sahoo, *Phys. Rev. C* **107**, 014910 (2023).
- [77] M. I. Gorenstein, *Phys. Rev. C* **86**, 044907 (2012).
- [78] K. Redlich, J. Cleymans, H. Satz, and E. Suhonen, *Nucl. Phys. A* **566**, 391 (1994).
- [79] A. Chodos, R. L. Jaffe, K. Johnson, C. B. Thorn, and V. F. Weisskopf, *Phys. Rev. D* **9**, 3471 (1974).
- [80] T. DeGrand, R. L. Jaffe, K. Johnson, and J. Kiskis, *Phys. Rev. D* **12**, 2060 (1975).
- [81] J. Cleymans, R. Gavai, and E. Suhonen, *Physics Reports* **130**, 217 (1986).
- [82] G. P. Kadam and H. Mishra, *Phys. Rev. C* **93**, 025205 (2016).
- [83] P. Koch, B. Müller, and J. Rafelski, *Physics Reports* **142**, 167 (1986).
- [84] P. Alba, W. Alberico, R. Bellwied, M. Bluhm, V. Manto-vani Sarti, M. Nahrgang, and C. Ratti, *Phys. Lett. B* **738**, 305 (2014).
- [85] S. Bhattacharyya, D. Biswas, S. K. Ghosh, R. Ray, and P. Singha, *Phys. Rev. D* **101**, 054002 (2020).
- [86] I. Bashir, R. A. Parra, H. Nanda, and S. Uddin, *Advances in High energy Physics* **9285759**, 1 (2018).
- [87] J. Cleymans, H. Oeschler, K. Redlich, and S. Wheaton, *Phys. Rev. C* **73**, 034905 (2006).
- [88] M. Mishra and C. P. Singh, *Phys. Rev. C* **78**, 024910 (2008).
- [89] J. Cleymans, H. Oeschler, K. Redlich, and S. Wheaton, *J. Phys. G: Nucl. Part. Phys.* **32**, S165 (2006).
- [90] S. Tiwari and C. P. Singh, *Advances in High energy Physics* **805413**, 1 (2013).
- [91] I. Bashir, H. Nanda, and S. Uddin, *Journal of Experimental and Theoretical Physics* **122**, 1032 (2016).
- [92] G. P. Kadam and H. Mishra, *Phys. Rev. D* **100**, 074015 (2019).
- [93] F. Becattini, J. Manninen, and M. Gaździcki, *Phys. Rev. C* **73**, 044905 (2006).
- [94] J. Cleymans and H. Satz, *Z. Phys. C* **57**, 135 (1993).
- [95] A. Khuntia, S. K. Tiwari, P. Sharma, R. Sahoo, and T. K. Nayak, *Phys. Rev. C* **100**, 014910 (2019).
- [96] J. Beringer *et al.*, *Phys. Rev. D* **86**, 010001 (2012).
- [97] L. Adamczyk *et al.* (STAR Collaboration), *Phys. Rev. C* **96**, 044904 (2017).
- [98] A. Rossi, G. Vannini, A. Bussière, E. Albini, D. D'Alessandro, and G. Giacometti, *Nuclear Physics B* **84**, 269 (1975).
- [99] M. M. Aggarwal *et al.* (STAR Collaboration), *Phys. Rev. C* **83**, 024901 (2011).
- [100] J. Adams *et al.* (STAR Collaboration), *Physics Letters B* **567**, 167 (2003).
- [101] E. Abbas *et al.* (The ALICE Collaboration), *Eur. Phys. J. C* **73**, 2496 (2013).
- [102] L. Ahle *et al.* (E802 Collaboration), *Phys. Rev. C* **60**, 064901 (1999).
- [103] B. I. Abelev *et al.* (STAR Collaboration), *Phys. Rev. C* **81**, 024911 (2010).
- [104] J. Adam *et al.* (STAR Collaboration), *Phys. Rev. C* **102**, 034909 (2020).
- [105] A. Mischke *et al.* (NA49 Collaboration), *J. Phys. G: Nucl. Part. Phys.* **28**, 1761 (2002).
- [106] C. Adler *et al.* (STAR Collaboration), *Phys. Rev. Lett.* **87**, 262302 (2001).
- [107] W. Broniowski and W. Florkowski, *Phys. Lett. B* **490**, 223 (2000).
- [108] W. Broniowski, W. Florkowski, and L. Ya. Glozman, *Phys. Rev. D* **70**, 117503 (2004).
- [109] B. Abelev *et al.* (ALICE Collaboration), *Phys. Rev. C* **88**, 044910 (2013).
- [110] J. Adams *et al.* (STAR Collaboration), *Phys. Rev. Lett.* **90**, 172301 (2003).
- [111] S. Pratt and C. Plumberg, *Phys. Rev. C* **104**, 014906 (2021).
- [112] B. I. Abelev *et al.* (STAR Collaboration), *Physics Letters B* **690**, 239 (2010).
- [113] J. Rafelski and B. Müller, *Phys. Rev. Lett.* **48**, 1066 (1982).

- [114] S. Pal, C. M. Ko, and Z.-w. Lin, [Phys. Rev. C \*\*64\*\*, 042201 \(2001\)](#).
- [115] S. A. Bass, A. Dumitru, M. Bleicher, L. Bravina, E. Zabrodin, H. Stöcker, and W. Greiner, [Phys. Rev. C \*\*60\*\*, 021902 \(1999\)](#).
- [116] C. Alt *et al.* (NA49 Collaboration), [Phys. Rev. C \*\*77\*\*, 024903 \(2008\)](#).
- [117] F. Wang, H. Liu, H. Sorge, N. Xu, and J. Yang, [Phys. Rev. C \*\*61\*\*, 064904 \(2000\)](#).
- [118] J. Kapusta and A. Mekjian, [Phys. Rev. D \*\*33\*\*, 1304 \(1986\)](#).
- [119] K. S. Lee, M. J. Rhoades-Brown, and U. Heinz, [Phys. Rev. C \*\*37\*\*, 1452 \(1988\)](#).
- [120] L. McLarren, [Rev. Mod. Phys. \*\*58\*\*, 1021 \(1986\)](#).
- [121] J. Rafelski, J. Letessier, and G. Torrieri, [Phys. Rev. C \*\*65\*\*, 069902 \(2002\)](#).
- [122] C. Blume and C. Markert, [Progress in Particle and Nuclear Physics \*\*66\*\*, 834 \(2011\)](#).
- [123] J. K. Nayak, S. Banik, and J.-e. Alam, [Phys. Rev. C \*\*82\*\*, 024914 \(2010\)](#).
- [124] J. Cleymans, H. Oeschler, K. Redlich, and S. Wheaton, [Eur. Phys. J. A \*\*29\*\*, 119 \(2006\)](#).
- [125] W. Busza and A. S. Goldhaber, [Phys. Lett. B \*\*139\*\*, 235 \(1984\)](#).
- [126] F. Wang, [Phys. Lett. B \*\*489\*\*, 273 \(2000\)](#).
- [127] F. Wang and N. Xu, [Phys. Rev. C \*\*61\*\*, 021904\(R\) \(2000\)](#).